The function of glutamatergic synapses is not perturbed by severe knockdown of 4.1N and 4.1G expression

Christian Wozny[1],[*],[‡],[§], Jörg Breustedt[1],[*], Friederike Wolk[2], Frédérique Varoqueaux[2], Susann Boretius[3], Aleksandar R. Zivkovic[1], Antje Neeb[4], Jens Frahm[3], Dietmar Schmitz[1], Nils Brose[2] and Aleksandra Ivanovic[2],[‡]

[1]Neuroscience Research Center, Charité–Universitätsmedizin Berlin, Charitéplatz 1, D-10117 Berlin, Germany
[2]Max-Planck-Institut für Experimentelle Medizin, Abteilung Molekulare Neurobiologie, DFG Center for Molecular Physiology of the Brain, Hermann-Rein-Str. 3, D-37075 Göttingen, Germany
[3]Biomedizinische NMR Forschungs GmbH, Max-Planck-Institut für Biophysikalische Chemie, Am Fassberg 11, D-37077 Göttingen, Germany
[4]Institut für Toxikologie und Genetik, Forschungszentrum Karlsruhe, Hermann-von-Helmholtz-Platz 1, D-76344 Eggenstein-Leopoldshafen, Germany
*These authors contributed equally to this work
‡Authors for correspondence (e-mails: ivanovic@em.mpg.de; cwozny@mrc-lmb.cam.ac.uk)
§Present address: MRC Laboratory of Molecular Biology, Hills Road, Cambridge CB2 0QH, UK

Summary

AMPA-type glutamate receptors mediate fast excitatory synaptic transmission in the vertebrate brain. Their surface expression at synapses between neurons is regulated in an activity-dependent and activity-independent manner. The protein machinery that regulates synaptic targeting, anchoring and turnover of AMPA receptors consists of several types of specialized scaffolding proteins. The FERM domain scaffolding proteins 4.1G and 4.1N were previously suggested to act jointly in binding and regulating synaptic trafficking of the AMPA receptor subunits GluR1 and GluR4. To determine the functions of 4.1G and 4.1N in vivo, we generated a mutant mouse line that lacks 4.1G entirely and expresses 4.1N at 22% of wild-type levels. These mice had combined 4.1G and 4.1N protein expression in the hippocampus at 12% of wild-type levels (equivalent to 8-10% of combined GluR1 and GluR4 expression levels). They show a moderate reduction in synaptosomal expression levels of the AMPA receptor subunit GluR1 at 3 weeks of age, but no change in basic glutamatergic synaptic transmission and long-term potentiation in the hippocampus. Our study indicates that 4.1G and 4.1N do not have a crucial role in glutamatergic synaptic transmission and the induction and maintenance of long-term plastic changes in synaptic efficacy.

Supplementary material available online at
http://jcs.biologists.org/cgi/content/full/122/5/735/DC1

Key words: Knockout, Mouse, Hippocampus, GluR1, GluR4, Synaptic plasticity

Introduction

The excitatory neurotransmitter glutamate activates α-amino-3-hydroxy-5-methylisoxazole-4-propionic acid (AMPA) receptors, N-methyl-D-aspartate (NMDA) receptors and kainate receptors. Fast excitatory transmission in the brain is mainly mediated by AMPA receptors (AMPARs), and its dynamic alteration is thought to be involved in several cognitive processes, including learning and memory.

One of the most extensively studied models of activity-dependent plastic changes in synaptic strength is long-term potentiation (LTP), which is thought to be crucial for learning and memory. NMDA-type receptors (NMDARs) are important for the induction of LTP, which involves long-lasting changes in synaptic strength caused by activity-dependent modulation of AMPAR-mediated transmission (Malenka and Bear, 2004). In the course of LTP generation, high-frequency stimuli activate AMPARs and NMDARs, leading to subsequent changes in trafficking of AMPARs to the synapse (Barry and Ziff, 2002; Bredt and Nicoll, 2003; Collingridge et al., 2004).

Several scaffolding proteins are known to regulate AMPAR trafficking, including the transmembrane AMPAR-regulatory proteins (TARPs), the ATPase N-ethylmaleimide-sensitive factor (NSF), members of the membrane-associated guanylate kinase

protein-family (MAGUKs) and other PDZ-domain-containing proteins, such as the glutamate receptor-interacting protein (GRIP) or the protein kinase C α (PKCα)-binding protein PICK1. Stargazin (CCG2) and γ-8 (CCG8) are members of the TARP family and were shown to be essential for the surface expression and clustering of AMPARs at synapses (Nicoll et al., 2006). Stargazin-deficient mice lack synaptic AMPARs in cerebellar granule cells, but show normal synaptic transmission in the hippocampus (Chen et al., 2000). In γ-8-knockout mice, hippocampal synaptic transmission and plasticity are reduced (Rouach et al., 2005). Overexpression of the MAGUK PSD95 increases AMPAR-mediated transmission (Beique and Andrade, 2003; Ehrlich and Malinow, 2004; Nakagawa et al., 2004; Schnell et al., 2002), and PSD93 PSD95 double-knockout mice show a severe impairment in fast excitatory transmission (Elias et al., 2006). GRIP, NSF and PICK1 interact directly with the cytoplasmic tail of the GluR2 subunit of AMPARs (Kim et al., 2001; Luthi et al., 1999; Setou et al., 2002).

The founding member of the protein 4.1 family, 4.1R (official mouse protein symbol, Epb4.1), was originally identified as a stabilizer of erythrocyte shape, connecting the transmembrane protein glycophorin C (GLPC) and the MAGUK p55 with the spectrin cytoskeleton (Marfatia et al., 1995). In addition to 4.1R,

the 4.1 family includes the members 4.1B (Epb4.1L3), 4.1G (Epb4.1L2) and 4.1N (Epb4.1L1). All four 4.1 proteins share a highly conserved domain structure characterized by the presence of an N-terminal FERM (four point one, ezrin, radixin, moesin) domain, a spectrin-actin-binding domain and a C-terminal domain, all of which interact with multiple transmembrane proteins. The ability of 4.1 proteins to bind very structurally diverse interaction partners via their different protein domains enables them to participate in many different physiological processes in a variety of cell types and tissues.

Proteins 4.1G and 4.1N have been shown to be expressed in neuronal and non-neuronal cells in the brain (Lu et al., 2004; Ohara et al., 2000; Ohno et al., 2005). Protein interactions with the GluR1 and GluR4 subunits of AMPARs were described for the MAGUK SAP97 and the 4.1 proteins 4.1N and 4.1G (Cai et al., 2002; Coleman et al., 2003; Rumbaugh et al., 2003; Shen et al., 2000). The *Drosophila* 4.1 protein homologue coracle interacts with GluRIIA (Chen et al., 2005) and binding of 4.1N and 4.1G is suggested to regulate surface expression of GluR1 and GluR4 (Coleman et al., 2003; Shen et al., 2000).

In the present study, we examined the role of the 4.1 paralogues 4.1G and 4.1N in hippocampal neurotransmission and synaptic plasticity using mutant mice in which combined 4.1N and 4.1G protein expression in the hippocampus is reduced to 12% of wild-type levels, which is equivalent to 8-10% of combined GluR1 and GluR4 expression levels.

Results

Targeting of the mouse 4.1G and 4.1N genes

The 4.1G and 4.1N double-mutant (4.1G/N) mice (abbreviated as DKO in figures) were generated by a conditional mutagenesis strategy. In both cases, two LoxP sites flanking the first coding exon and a neomycin-resistance gene flanked by frt sites were introduced by homologous recombination in embryonic stem cells (129/ola) (Fig. 1A,D). A fragment representing bp 25,131,023-25,131,494 on band A3 of Chromosome 10 and bp 1-471 in the 4.1G mRNA (AJ542537) was floxed in the mouse 4.1G gene *Epb4ll2* (GeneID 13822). The 4.1N gene *Epb4ll1* (GeneID 13821) is located on band H2 of Chromosome 2. The region representing bp 156,185,360-156,185,551 in the 4.1N gene and bp 206-396 in 4.1N mRNA (AF061283) was floxed. Of 192 screened embryonic stem (ES) cell clones in both cases, nine clones with the desired 4.1G recombination and 15 clones with the desired 4.1N recombination were identified by Southern blot analysis with a 5′ external probe (probe 1 for 4.1G, Fig. 1A; probe 2 for 4.1N, Fig. 1D). Two ES cell clones of each gene were injected into C57BL/6 blastocysts. The offspring of chimeric males and subsequent generations were genotyped by PCR (Fig. 1C,F,G). The resulting recombinant single 4.1G$^{+/-}$ and 4.1N$^{+/-}$ mice were bred with EIIaCre deleter mice (Lakso et al., 1996), which resulted in the loss of the first coding exon in both cases (Fig. 1G). The 4.1G-knockout mice were then crossed with 4.1N mutant mice to breed 4.1G/N double-mutant animals. The offspring were bred to homozygosity and selected for the absence of the *Cre* transgene.
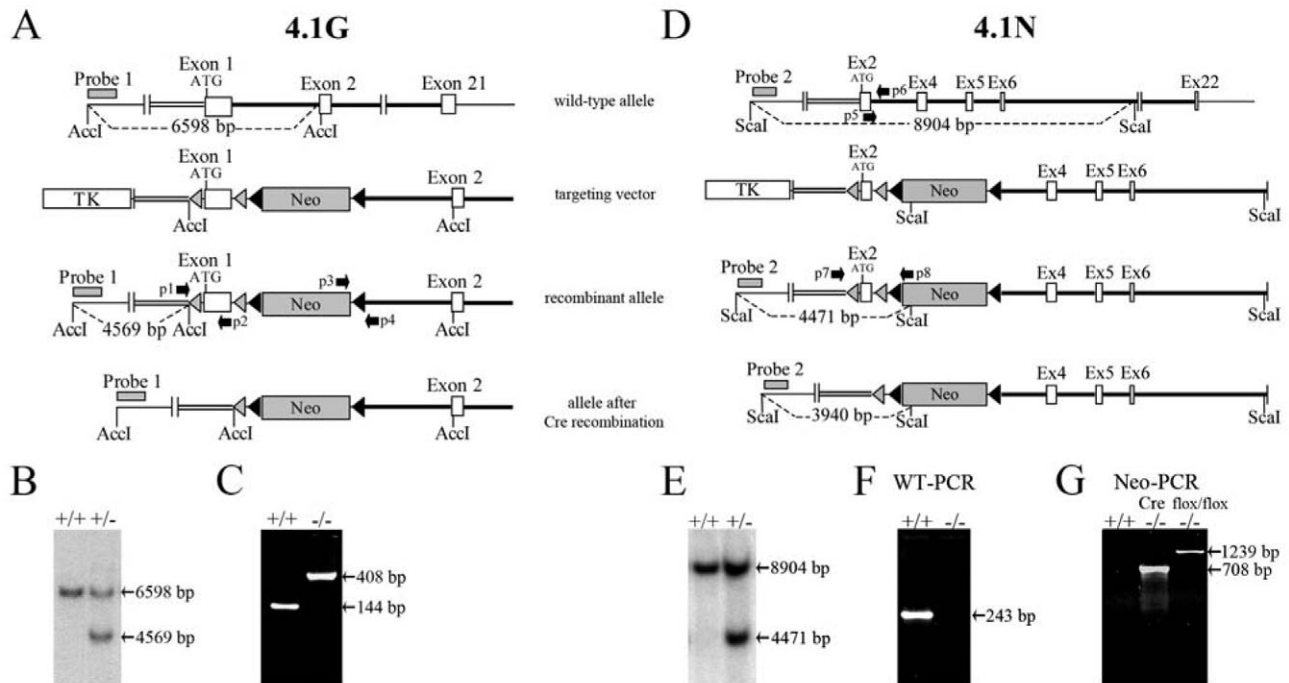

Fig. 1. Targeting of genes encoding 4.1G and 4.1N. (A,D) Schematic representations of the mouse 4.1G and 4.1N genomic loci, targeting vectors, targeted alleles, and excision of the first coding exon by Cre recombinase. LoxP sites are indicated by grey triangles, the neomycin selection cassette is flanked by frt sites (black arrowheads) for possible excision by flip recombinase. Ex, exon. (A) Targeting strategy for gene encoding 4.1G. The first coding exon has been excised. The positions of *Acc*I restriction sites and the 5′ Southern probe (Probe 1) are shown. (B) Southern blot analysis of 4.1G. Probe P1 was used for hybridisation. The signal for the 4.1G WT allele resulted in a 6598 bp band and the recombinant allele resulted in a 4569 bp band. (C) Genotyping of 4.1G WT and mutant mice by PCR. In 4.1G WT animals primers p1 and p2 generated a 144 bp band. In recombinant alleles and after Cre recombination a 408 bp fragment is synthesized with primers p3 and p4. (D) Targeting strategy for gene encoding 4.1N. The first coding exon has been excised. The positions of *Sca*I restriction sites and the 5′ Southern probe (Probe 2) are marked. (E) Southern blot analysis with Probe 2 after *Sca*I digestion of stem cell DNA. The introduction of the neomycin selection cassette resulted in an additional *Sca*I restriction site and a shift of the 8904 bp WT band to a 4471 bp band. (F,G) Genotyping of 4.1N mutants. Genotyping of mouse tail DNA with primers p5 and p6 resulted in a 243 bp WT band and no band was synthesized after knockout of 4.1N (F). In genomic PCRs with primers p7 and p8, a 1239 bp band for the recombinant allele (flox/flox$^{-/-}$) and a 708 bp band after Cre recombination (Cre$^{-/-}$) were detected (G).

Anatomy and cage behaviour of 4.1G/N double mutants

Neither single mutants nor homozygous 4.1G/N double mutants showed obvious phenotypic alterations. The 4.1G/N double-mutant mice were born at the expected mendelian frequency, and no gross behavioural abnormalities were apparent. The life spans were similar to those of control animals (data not shown).

Examination of the double-mutant animals by MRI using T1- and T2-weighted images showed only slight changes in the gross anatomy of the brain in 3-week-old animals (Fig. 2A). Quantitative volumetric analyses revealed mild, although significant, reductions in whole brain volume and cerebellar volume in young 4.1G/N double-mutant mice (Fig. 2C,D). These changes seem to be compensated during development, as they were absent in 7-month-old double-mutant mice (Fig. 2B-E).

Immunohistochemical staining was performed to determine the number of matched and mismatched pre- and postsynaptic components of glutamatergic synapses in the stratum radiatum of hippocampal CA1 area of 4.1G/N double mutants and wild-type (WT) controls at the age of 3 weeks. Neither the spatial distribution nor the densities of puncta positive for VGLUT1/VGLUT2, ProSAP1 or both were altered significantly in 4.1G/N double-mutant hippocampus (Fig. 3A,B). Moreover, the ultrastructure of synapses formed in double-mutant animals was indistinguishable from that of WT controls (Fig. 3C). Mature synaptic specializations were observed in the CA1 region of 3-week-old mice in both the mutant and WT animals. Synaptic parameters, such as the number of synapses per 100 μm^2, the length of the postsynaptic density and the width of the postsynaptic density, were similar in both groups (Fig. 3D) (WT, $n=3$; DKO, $n=3$). Taken together, these data indicate

that the expression of proteins 4.1G and 4.1N is not critical for proper formation of glutamatergic synapses.

Expression of 4.1 proteins in 4.1G/N double-mutant mice

Western blot analyses confirmed that 4.1G was completely absent in 4.1G/N double-mutant mice (Fig. 4A), whereas the short variant of two 4.1N isoforms was still present (Fig. 4B; Fig. 5B,C), albeit reduced to a level of 30% of that in control preparations (Fig. 5D). The level of 4.1B protein was unchanged in the 4.1G/N double-mutant animals (supplementary material Fig. S1). The ratio between the short and the long variant of 4.1N in the hippocampus is 2.6±0.7 ($n=6$, calculated based on a densitometric analysis of the data shown in Fig. 5B,C). Thus, a 70% reduction of the short form of 4.1N and a complete elimination of the long 4.1N variant in our mutants is equivalent to a 78% reduction of total 4.1N expression in the hippocampus of 4.1N/G double-mutant mice. The ratio between 4.1N and 4.1G protein expression is 1:0.78 in rat total hippocampus (Yamakawa and Ohara, 2000) and 1:0.94 in mouse hippocampus postsynaptic density preparations (Trinidad et al., 2008). Thus, the reduction of combined 4.1G/N protein expression in our homozygous double-mutant hippocampus is estimated to be 88-89% compared with WT controls.

To deduce the primary structure of the residually expressed 4.1N isoform, we performed western blot analyses with three domain-specific antibodies: anti-4.1N exon 2 directed against the first 15 amino acids encoded by exon 2, anti-4.1N monoclonal antibody (BD Biosciences), which is specific for a region of the spectrin-actin-binding domain, and an anti-CTD antibody against the C-terminal domain of 4.1N (Fig. 5E). Fig. 5A shows that the anti-
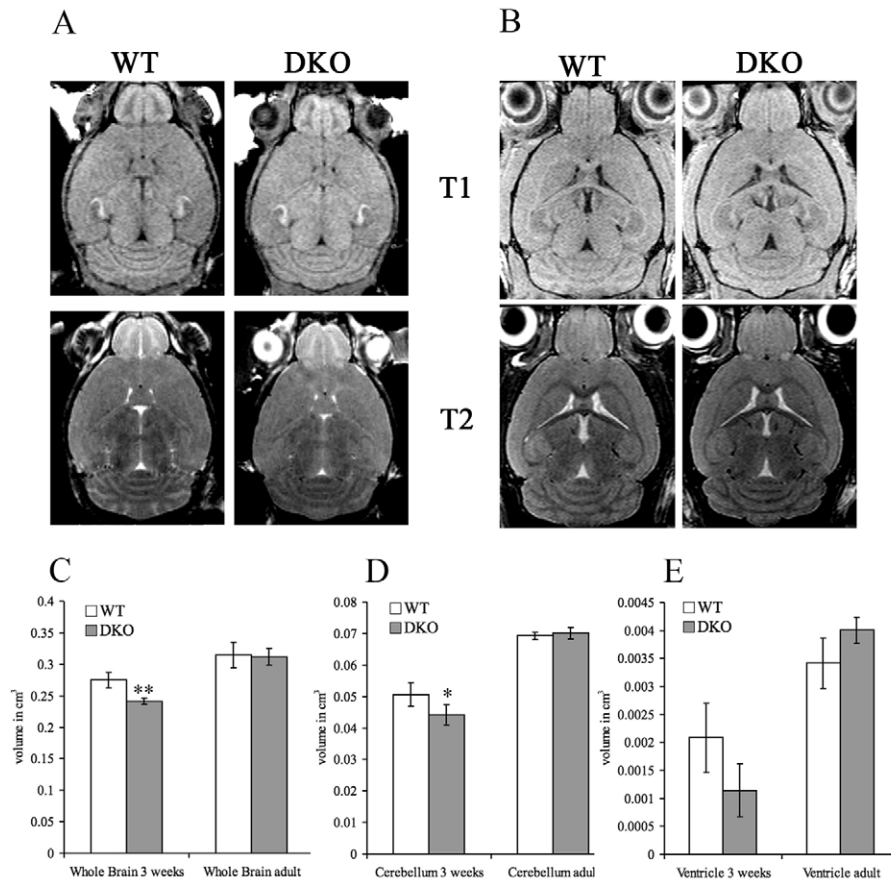
Fig. 2. Anatomical differences in young 4.1G/N double-mutant mice are compensated during development. (A) Anatomical 3D MRI at age 3 weeks. T1-weighted (upper panel) and T2-weighted (lower panel) horizontal sections from 3D MRI data sets of WT and 4.1G/N double-mutant (DKO) mice reveal no obvious differences in overall brain morphology ($n=4$, for WT and DKO). (B) 3D MRI of adult mice. T1-weighted (upper panel) and T2-weighted (lower panel) horizontal sections from 3D MRI data sets of WT and 4.1G/N double-mutant mice reveal no obvious differences in overall brain morphology ($n=3$, for WT and DKO). (C) Quantitative in vivo MRI volumes based on the images shown in A, error bars indicate s.d. The whole-brain volume was significantly reduced in the 4.1G/N double mutants at the age of 3 weeks (**$P=0.0074$, determined by Student's t-test) but not in adult mutants. (D) The cerebellar volume was significantly reduced in the 4.1G/N double mutants at the age of 3 weeks (*$P=0.039$, determined by Student's t-test, error bars indicate s.d.) but not in adult mutants. (E) The ventricle volume was not altered in 3-week-old 4.1G/N double-mutant or in adult mice.
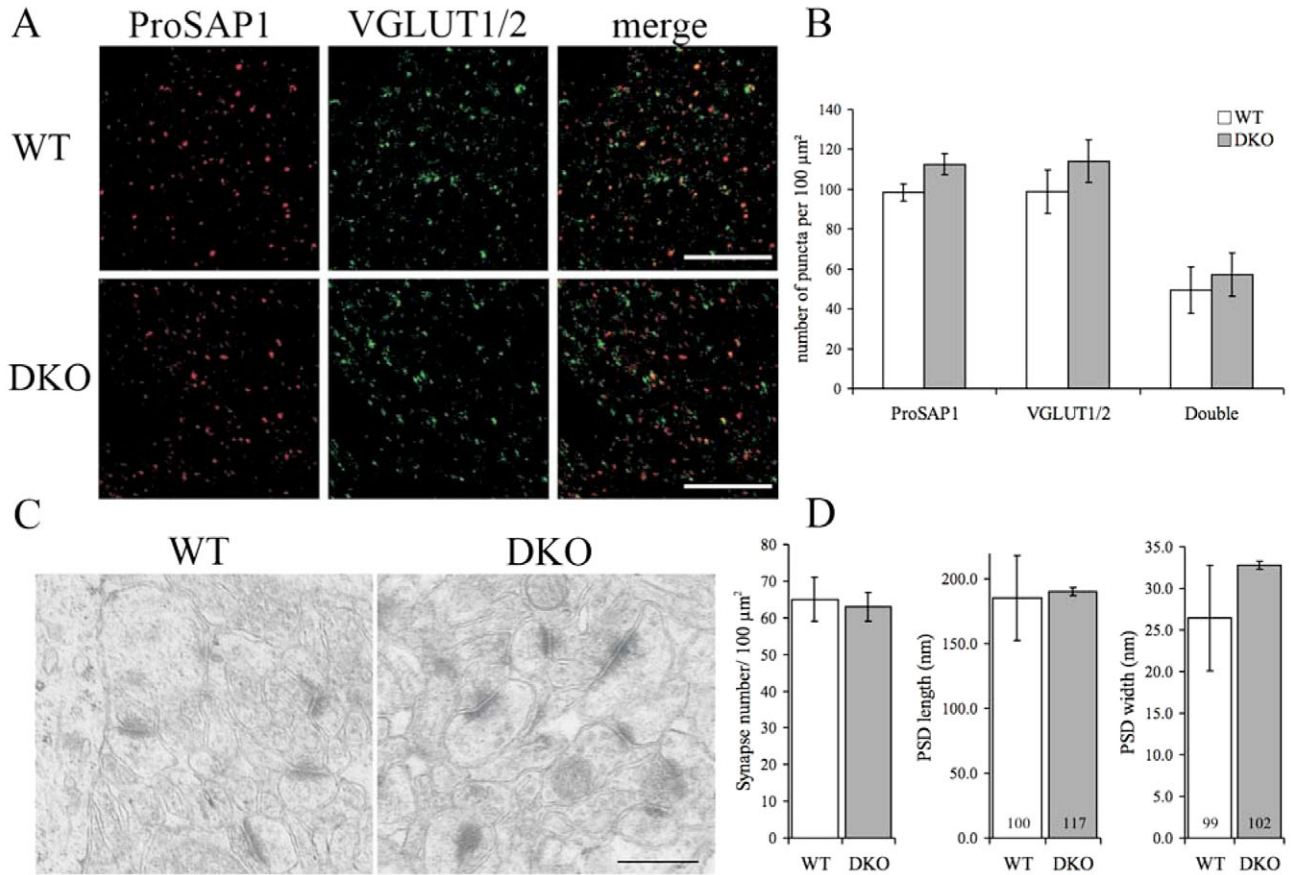
Fig. 3. Synaptic morphology in the hippocampus of 4.1G/N double-mutant mice. (A) Properly aligned pre- and postsynaptic specializations in stratum radiatum of hippocampal area CA1. The left panel shows representative micrographs of the CA1 area of control (WT, n=3) and 4.1G/N double-mutant (DKO, n=3) sections after double labeling for glutamatergic excitatory postsynapses (stained for ProSAP1, red) and presynapses (stained for VGLUT1/2, green). Scale bars: 8 μm. (B) Quantification of isolated and colocalized ProSAP1 and VGLUT1/2 puncta in the CA1 region of control (WT, white, n=3) and 4.1G/N double-mutant mice (DKO, grey, n=3). The total numbers of synapses were not significantly different in the two experimental groups. Error bars indicate s.d. (C,D) Ultrastructural analysis of CA1 neurons in 4.1G/N double-mutant mice and WT controls at the age of 3 weeks. Mature synaptic specializations were observed in both groups; quantification was performed in the stratum radiatum. The number of synapses per 100 μm^2 and the length and the width of PSDs were similar in both experimental groups. Error bars indicate s.d. The numbers within the bars in D indicate the number of synapses. Scale bar: 500 nm.

4.1N exon 2 antibody detected only the upper band in the WT, whereas in the 4.1G/N double-mutant mice, no signal was recognized at all (n=3). By contrast, the anti-4.1N monoclonal antibody and the anti-4.1N CTD antibodies detected two bands in the WT, whereas only the lower band was identified in the 4.1G/N double mutants (n=3) (Fig. 5B,C).

To characterize the residual 4.1N splicing variant in the 4.1G/N double mutants, we combined RACE (rapid amplification of cDNA ends) experiments and database analyses. The disappearance of the lower WT 4.1N band in western blots stained with the anti-4.1N exon 2 antibody (Fig. 5A, left panel) indicated an alternative use of the first coding exon, as previously reported for 4.1R and 4.1B (Conboy, 1991; Gascard, 2004). There are indications of alternative start codon use in human (NM_177966) and equine (XM_001501911) 4.1N mRNA, but no corresponding 4.1N mRNA or ESTs could be identified for the mouse.

To define the full brain-specific use of 4.1N exons in WT and 4.1G/N double mutants, we generated 5′RACE and 3′RACE transcript sequences (Fig. 5G). All transcripts cloned experimentally by 5′RACE from WT (12 clones) included exon 2. Exon 3 never contributed to the 5′RACE sequences in the WT.

The 3′ RACE-PCRs generated two different populations of transcripts. Four of nine clones encoded the high molecular weight class of 4.1N including exon 17B. The other five clones corresponded to the lower 4.1N form. To our surprise, in the 4.1G/N double mutants all 5′RACE-PCR transcripts (nine clones) started with exon 3, which is usually removed from mature mRNA, and the first initiation codon was localized in exon 4. All 3′RACE PCR clones from the 4.1G/N double mutants lacked exon 17A and exon 17B. As the anti-4.1N exon 2 peptide antibody is directed against the first 15 amino acids of the N-terminus, it is possible that this epitope is not accessible for the antibody in the WT 4.1N short variant. The absence of a band in the 4.1G/N double mutants can be explained by the genetic knockout of exon 2, which includes the epitope of the anti-4.1N exon 2 antibody. We conclude from the results obtained by western blots and RACE experiments that the residually expressed protein in 4.1G/N double mutants is similar to the short form expressed in the WT, but differs in its N-terminal sequence.

Next, we determined expression levels of GluR1, GluR2/3, GluR4 and NR1 in young adult 4.1G/N double-mutant mice by quantitative western blot analyses of synaptosome preparations from
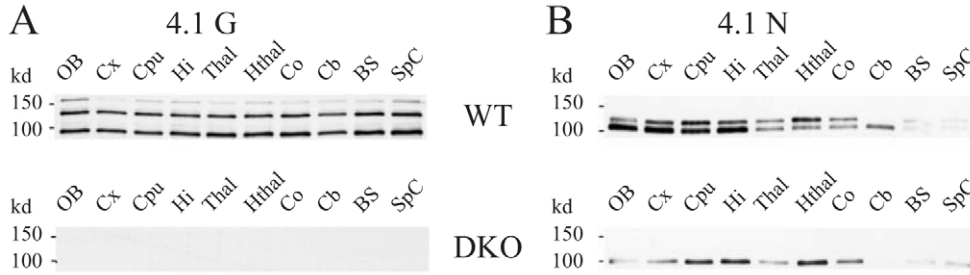
Fig. 4. Expression pattern of 4.1G and 4.1N in WT and 4.1G/N double-mutant brains. (A) Western blot analysis using a 4.1G-specific antibody detecting an epitope located within the first coding exon. 4.1G is expressed in all examined regions of the central nervous system (upper panel). OB, olfactory bulb; CX, cortex; CPu, striatum; Hi, hippocampus; Thal, thalamus; Hthal, hypothalamus; Co, colliculus; Cb, cerebellum; BS, brain stem; SpC, spinal cord. No signal was detected in 4.1G/N double-mutant mice (lower panel). (B) Western blot analysis using the 4.1N monoclonal antibody. 4.1N is expressed in all examined brain regions with minor expression in BS and SpC. The short variant of the two 4.1N isoforms was still present at low levels in the 4.1G/N double-mutant animals.

whole-brain homogenates (Fig. 6A). Here, we found significantly reduced synaptic GluR1 protein levels in synaptosomes from 4.1G/N double-mutant mice (WT, $n=6$; DKO, $n=6$; **$P<0.01$). Furthermore, we measured GluR1, GluR2/3 and GluR4 concentrations in Triton-X-100-insoluble postsynaptic density (PSD) preparations of hippocampi obtained from young adult 4.1G/N double-mutant mice and WT controls. Supporting our findings in synaptosomes, we found significant changes in the levels of the GluR1 subunit (Fig. 6B) (WT, $n=7$; DKO, $n=7$; *$P<0.05$). GluR2/3 levels were also significantly decreased in PSD preparations, although a direct interaction between 4.1G or 4.1N and GluR2/3 has not been described. In vivo, AMPARs usually form heteromers composed of different subunits. A reduction in the

GluR1 subunit might therefore be accompanied by a reduction of other GluR subunits such as GluR2/3.

Synaptic and extrasynaptic AMPAR responses are normal in young 4.1G/N double-mutant mice

The Schaffer collateral synapses in the hippocampus are very well characterized with respect to their short- and long-term synaptic plasticity. It is generally accepted that the induction of long-term potentiation (LTP) in area CA1 is NMDAR dependent (Malenka and Bear, 2004). A leading hypothesis states that LTP in area CA1 is activity dependent and relies on insertion of AMPARs as GluR1/GluR2-containing receptors are driven into the synapses after the induction of LTP (Hayashi et al., 2000).
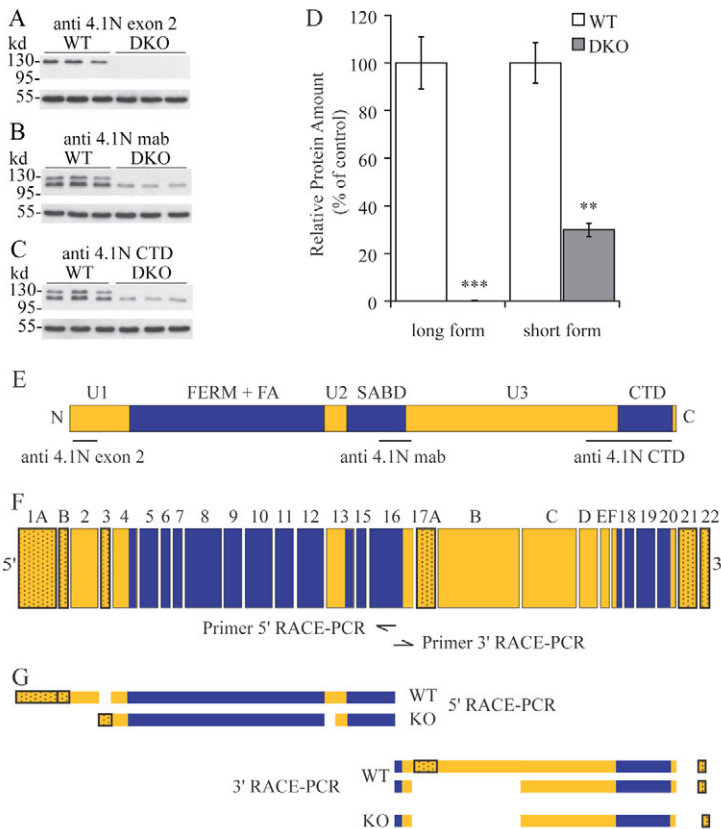

Fig. 5. Residual expression of a shorter 4.1N form in the 4.1G/N double-mutant hippocampus. (A-C) Hippocampal preparations from 3-week-old WT (left panel) or 3-week-old 4.1G/N double mutant (right panel) were loaded and stained on western blots with the following antibodies. (A) Anti-4.1N exon 2, which is directed against the first 15 amino acids of the N-terminus; (B) Anti-4.1N monoclonal antibody, which recognizes a C-terminal region of the spectrin-actin-binding domain; (C) Anti-4.1N CTD, which is detecting the very C-terminus of 4.1N. (D) Densitometric quantification of data pooled from B and C. The error bars indicate s.e.m. **$P<0.01$; ***$P<0.001$; Student's t-test. (E) Schematic representation of the murine full-length 4.1N protein. The positions of the epitopes of the antibodies used in A-C are indicated. U1, unique region 1; FERM, Four-point-one, ezrin, radixin, moesin homology domain; FA, FERM adjacent region; U2, unique region 2; SABD, spectrin-actin-binding domain; U3, unique region 3; CTD, C-terminal domain. Unique regions are shown in yellow, conserved areas are in blue. (F) Exon usage map of the mouse 4.1N gene in brain. Numbering is derived from mouse *Epb41l1* as described (Ramez et al., 2003). The colour code is modelled on the domain structure shown in E. Dotted boxes denote nontranscribed exons. The positions of the specific 5′RACE primers and the specific 3′RACE primers are indicated by arrows. (G) Schematic representation of the obtained RACE transcripts from WT and 4.1G/N double mutants.
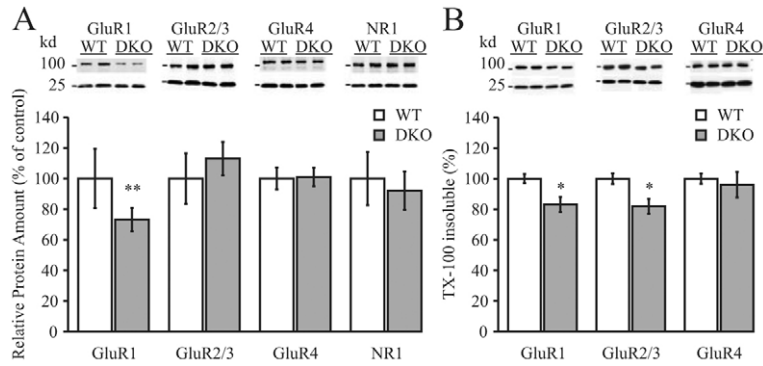
Fig. 6. GluR levels are altered in 4.1G/N double-mutant mice. (A) Reduced GluR1 levels in whole brain synaptosomal preparations. Protein levels in synaptosomal fractions of 3-week-old mice expressed as percentage of WT levels. Error bars indicate s.d. (WT, *n*=6; DKO, *n*=6; ***P*<0.01). (B) Reduced GluR1 and GluR2/3 levels in PSD preparations from young adult hippocampi. Protein levels are expressed as percentage (± s.d.) of WT levels (WT, *n*=7; DKO, *n*=7; **P*<0.05).

As 4.1 proteins were shown to interact with the GluR1 subunit and because we found a reduction of GluR1 expression in synaptosomes of 4.1G/N double-mutant mice (Fig. 6A), we tested whether the loss of protein 4.1G together with the strong reduction of protein 4.1N leads to alterations in synaptic transmission and changes in LTP in young adult 4.1G/N double mutants. To measure synaptic responses in hippocampal brain slices of 4.1G/N double-mutant mice, we stimulated the Schaffer collaterals in area CA1 and recorded postsynaptic field potentials (fEPSPs) in the stratum radiatum of area CA1. Comparing the size of the presynaptic afferent volley (representative of presynaptic excitability), with the slope of the fEPSP (representing postsynaptic responsiveness), we found no significant differences in the fEPSP slopes at various afferent volley amplitudes (WT, *n*=10; DKO, *n*=13) (Fig. 7A). Using whole-cell patch-clamp recordings, we found that the ratio of AMPAR- to NMDAR-mediated excitatory postsynaptic current (EPSC) is not altered in 4.1G/N double mutants (AMPA/NMDA ratio: WT, 4.8±0.9, *n*=13; DKO, 6.1±1.1, *n*=11; *P*=0.39; AMPAR-mediated EPSC: WT, 241±20 pA; DKO, 281±26 pA, *P*=0.23; NMDAR-mediated component: WT, 66±10 pA; DKO, 54±9 pA, *P*=0.35) (Fig. 7B).

Paired-pulse facilitation (PPF) is a form of short-term plasticity and generally assumed to be of presynaptic origin. Using a paired-pulse stimulation protocol, the second response is facilitated compared with the first response within a short time-window. Using different stimulation intervals varying from 50 mseconds to 500 mseconds, we found that PPF in field recordings is not significantly changed in 4.1G/N double mutants (WT, 1.44±0.06, *n*=7; DKO, 1.39±0.03, *n*=10; *P*=0.4). Whole-cell recordings confirmed these data at an interstimulus interval of 50 mseconds (WT PPF, 1.47±0.07, *n*=15; DKO PPF, 1.47±0.04, *n*=15; *P*=0.97) (Fig. 7C,D). We also recorded miniature EPSCs (mEPSCs) in the presence of the sodium channel blocker tetrodotoxin (TTX, 1 µM) and the AMPAR desensitization inhibitor cyclothiazide (CTZ, 100 µM). AMPAR-mediated mEPSCs showed neither a difference in frequency nor a difference in amplitude recorded at –60 mV between WT and 4.1G/N double-mutant animals. The mean mEPSC frequency was 0.9±0.1 Hz in WT mice and 1.2±0.1 Hz in 4.1G/N double mutants (WT, *n*=5; DKO, *n*=9; *P*=0.11) and the mean amplitude of the AMPAR-mediated mEPSCs was 18±2 pA in WT animals and 16±1 pA in 4.1G/N double-mutant mice (Fig. 8) (*P*=0.31). In summary, basal synaptic properties of
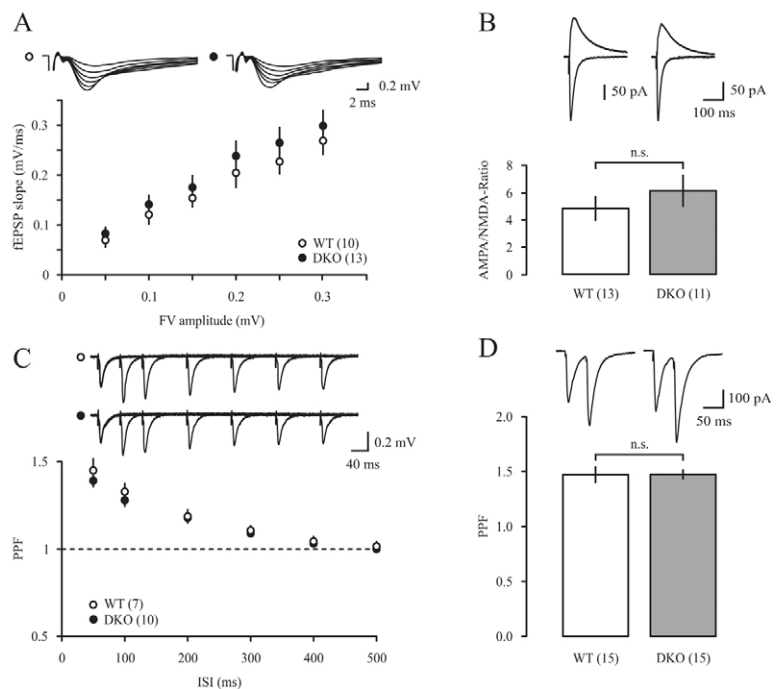

Fig. 7. Synaptic responses in area CA1 in WT and 4.1G/N double-mutant mice. (A) Input-output curves for basal synaptic transmission in area CA1 of the hippocampus. Sample traces are shown for the input (fiber volley) and the output (fEPSP). No significant difference was found between WT and 4.1G/N double mutants in the fEPSP slopes at various afferent volley amplitudes (WT, *n*=10; DKO, *n*=13). (B) Ratio of AMPA and NMDA currents is not altered in 4.1G/N double mutants (AMPA/NMDA ratio: WT, *n*=13; DKO, *n*=11). Sample traces from CA1 pyramidal cells are shown. (C) Paired-pulse facilitation (PPF) is unchanged in 4.1G/N double-mutant mice. PPF in field recordings is not significantly changed in double-mutant mice at intervals varying from 50 mseconds to 500 mseconds (WT, *n*=7; DKO, *n*=10). (D) Whole-cell recordings from CA1 pyramidal cells do not reveal differences in PPF between WT and 4.1G/N double mutants at an interstimulus interval of 50 mseconds (WT, *n*=15; DKO, *n*=15). Stimulus artefacts were removed.
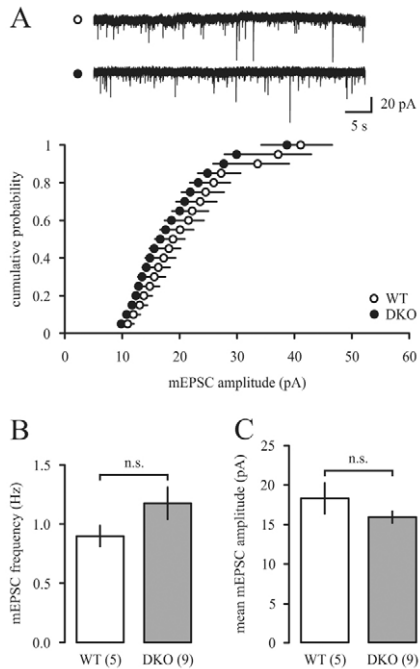
Fig. 8. mEPSCs recorded from CA1 pyramidal neurons in WT and 4.1G/N double-mutant animals. (A,B) Miniature EPSCs (mEPSCs) were recorded in the presence of the sodium channel blocker tetrodotoxin (TTX, 1 µM) and the AMPAR-desensitization inhibitor cyclothiazide (CTZ, 100 µM). mEPSCs showed no change in frequency (A) or amplitude (B). (C) Recordings of WT and 4.1G/N double mutants cells at –60 mV (for details see text). A cumulative frequency distribution of mEPSCs amplitudes is shown in (A). n.s., not significant.

AMPARs are not significantly changed in 4.1G/N double-mutant mice.

Next, we tested for alterations in the biophysical properties of AMPAR-mediated currents by measuring the rectification index, which was not significantly different between WT and 4.1G/N double-mutant neurons (2.8±0.4, n=6 and 2.7±0.4, n=6, respectively, P=0.8) (see supplementary material Fig. S2). Also, pharmacological challenging of AMPARs with the relatively selective GluR2 antagonist Naphthyl-acetyl-spermine (100 µM) revealed no differences in the slope of fEPSP recordings between the two genotypes (WT slope, 97.7±0.5% of control; DKO slope, 99.0±3% of control, n=4). The effectivity of the drug was confirmed by EPSC recordings from interneurons, where a substantial amplitude reduction was observed (see supplementary material Fig. S3). We thus did not find any indication for a change in AMPAR subunit composition in 4.1G/N double-mutant neurons.

As it is known that 4.1 proteins interact with AMPARs, we tested whether extrasynaptically located AMPAR are altered in 4.1G/N double-mutant mice. In the presence of TTX and CTZ, we bath-applied S-AMPA (100 nM) for 5 minutes and recorded the whole-cell current. By this procedure AMPARs are activated in the synaptic cleft, on the dendrites and on the somata. Application of S-AMPA led to a robust inward current of approximately 400-500 pA in WT and 4.1G/N double-mutant cells, with no significant differences between the tested genotypes (WT, 510±47 pA, n=4; DKO, 462±51 pA, n=5; P=0.52) (Fig. 9). Taken together, these results show that neither synaptic nor extrasynaptic AMPAR function is affected in 4.1G/N double mutants.
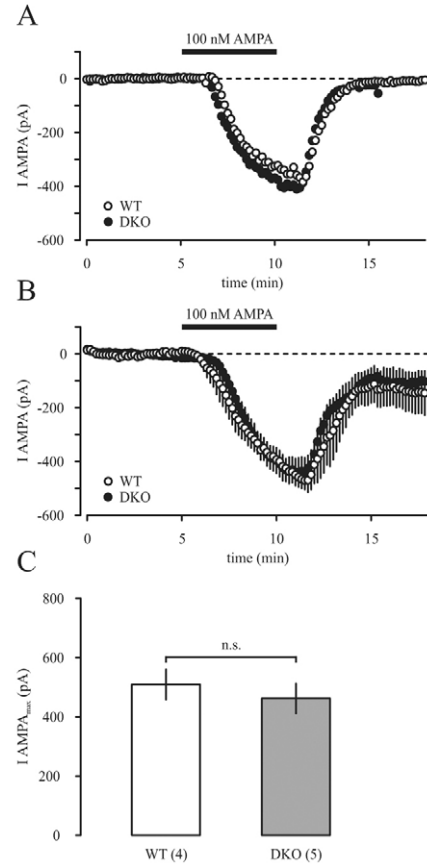

Fig. 9. Extrasynaptic AMPA currents are not reduced in 4.1G/N double-mutant mice. (A,B) Whole-cell currents evoked by bath application of 100 nM AMPA. A single example is shown in A and a summary plot in B. AMPA was applied for 5 minutes in the presence of 100 µM cyclothiazide and 1 µM TTX. (C) Maximal AMPA whole-cell current is not altered in 4.1G/N double mutants. The numbers in parentheses indicate the number of mice studied. n.s., not significant.

Long-term potentiation is normal in young 4.1G/N double-mutant mice

We studied long-term synaptic plasticity in WT and 4.1G/N double-mutant mice using field potential recordings. After recording stable fEPSPs in area CA1 for 10-20 minutes, the Schaffer collaterals were stimulated tetanically (four 1-second trains of 100 Hz, separated by 20 seconds). LTP was stable for 30-40 minutes after the tetanic stimulation in WT and 4.1G/N double mutants. No significant differences between WT and 4.1G/N double-mutant mice were found in the fEPSP slope 30-40 minutes after induction of LTP (Fig. 10) (WT, 137±6%, n=10; DKO, 135±7%, n=11; P=0.8). These data show that neither basal synaptic transmission nor short-term or long-term plasticity are altered in 4.1G/N double-mutant mice.

Discussion

In the present study, we used 4.1G/N double-mutant mice to assess the role of proteins 4.1G and 4.1N in glutamate receptor trafficking and synaptic anchoring, in hippocampal synaptic transmission and in synaptic plasticity. We found that (1) in young adult mice the GluR1 expression levels in 4.1G/N double mutants are reduced in synaptosomal and PSD fractions (Fig. 6); (2) GluR2/3 expression levels in 4.1G/N double mutants are reduced in PSD fractions (Fig. 6); (3) AMPAR-mediated glutamatergic synaptic transmission in
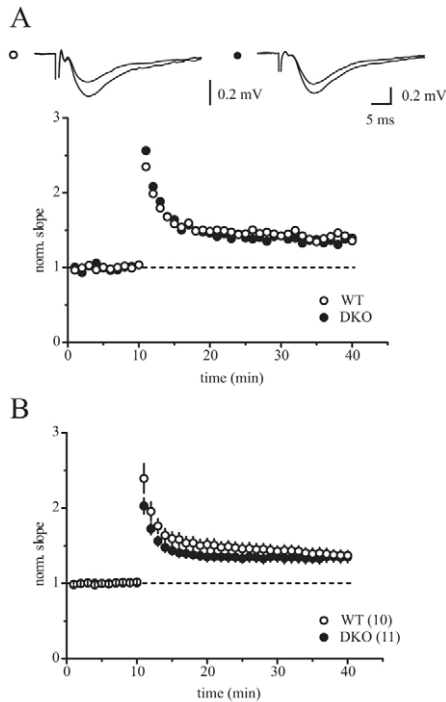
A

B

Fig. 10. LTP is not impaired in 4.1G/N double-mutant animals. (A) Depicted are representative results from WT (open circles) and 4.1G/N double-mutant (filled circles) animals. LTP was induced by tetanic stimulation, i.e. 100 pulses at 100 Hz, four 4 times, 20 seconds apart. Traces on top of the graph are averages of 7-10 consecutive responses each, taken from control and at the end of the recording period. (B) Summary plot of 10 experiments in WT and 11 experiments in 4.1G/N double-mutant mice. No differences in synaptic plasticity were detected between both groups.

4.1G/N double mutants is not changed (Figs 7-9), which is not consistent with the previously published notion that proteins 4.1G and 4.1N bind GluR1 and tether it to the postsynaptic cytoskeleton (Shen et al., 2000); and (4) LTP at CA3-CA1 Schaffer collaterals in 4.1G/N double mutants is not altered (Fig. 10), which argues against a crucial role of proteins 4.1G and 4.1N in the activity-dependent insertion of GluR1-containing AMPARs into potentiated synapses (Hayashi et al., 2000).

The two AMPA receptor subunits that were shown to bind 4.1 proteins, GluR1 and GluR4, bind to both 4.1N and 4.1G (Shen et al., 2000; Coleman et al., 2003). Thus, 4.1N and 4.1G can be viewed to have a joint role in GluR1 and GluR4 trafficking. Our knockout strategy eliminated 4.1G expression entirely and 4.1N expression very strongly. The combined 4.1N/G protein expression in double-mutant hippocampus was reduced to 11-12% of WT levels. If 4.1G and 4.1N acted jointly as crucial stoichiometric interaction partners and scaffold proteins of GluR1 and GluR4 under normal circumstances, the residual expression of 4.1N in the 4.1G/N double-mutant mice is unlikely to be sufficient for the maintenance of normal function, because the relative expression levels of 4.1G, 4.1N, GluR1 and GluR4 in mouse hippocampus are 0.89-0.99, 0.95-1.05, 1.48-1.61, and 0.87-0.95, respectively (Trinidad et al., 2008). Thus, total deletion of 4.1G and a reduction of 4.1N expression by 78% would lead to a massively sub-stoichiometric ratio between combined 4.1G and 4.1N, and combined GluR1 and GluR4 expression in mouse hippocampus of at least 0.08:1, and 0.1:1, at most. Such a massive deficiency

of 4.1G and 4.1N expression compared with GluR1 and GluR4 expression in the double-mutant hippocampus would be expected to have severe functional consequences on glutamatergic transmission if 4.1G and 4.1N had a crucial role in GluR1 and GluR4 trafficking and anchoring, but our data show that this is not the case.

The fact that GluR1 levels are reduced in 4.1G/N double mutants supports the notion that proteins 4.1G and 4.1N bind GluR1 and stabilize it (Shen et al., 2000). However, the finding that neither basal AMPAR-mediated synaptic transmission nor synaptic plasticity in the hippocampus are altered in 4.1G/N double mutants makes an essential role of proteins 4.1N and 4.1G in the trafficking, function, and dynamics of AMPARs in vivo rather unlikely. This lack of phenotypic changes in 4.1G/N double mutants is either due to the fact that previously published in vitro experiments on the role of 4.1G and 4.1N in GluR1 trafficking and anchoring detected cell-culture specific phenotypes that are not relevant in vivo, or is caused by the fact that multiple AMPAR scaffold proteins operate in parallel at synapses and can substitute for the loss of the two scaffold proteins studied here. We favour the latter notion, as outlined below.

Striking functional redundancy has been reported for other postsynaptic AMPAR scaffold protein families that have been studied in detail. Targeted truncation of PSD95 in mutant mice, for example, does not affect AMPAR-mediated synaptic transmission in the hippocampus (Migaud et al., 1998). Similarly, single deletions of PSD95 or PSD93 do not cause functional changes in basal synaptic transmission (Elias et al., 2006). Only the simultaneous deletion of both PSD93 and PSD95 leads to marked reductions in glutamatergic synaptic transmission (Elias et al., 2006). By contrast, individual knockdown of either PSD93 or PSD95 using an shRNA strategy causes impaired glutamatergic transmission in hippocampal slice cultures (Elias et al., 2006). These findings indicate that PSD93 and PSD95 are functionally redundant and can compensate for the loss of the other MAGUK if sufficient time is available for these compensatory mechanisms to take place, as is the case in the deletion mutant mice, but apparently not when the proteins are knocked down by shRNAs.

Two recent studies found the interaction of stargazin and other TARPs with AMPARs to be the most robust and least transient compared with other putative interactions, including those with 4.1 proteins (Fukata et al., 2005; Vandenberghe et al., 2005). Indeed, TARPs function as auxiliary subunits of AMPARs and are important determinants of AMPAR trafficking and synaptic anchoring. An 80-90% reduction in hippocampal AMPAR protein levels and a 30-40% reduction in synaptic transmission are observed in γ-8-knockout mice, and extrasynaptic AMPARs were also reduced by 80-90% (Rouach et al., 2005). Similarly, cerebellar granule cells from mice lacking Stargazin lack synaptic and extrasynaptic AMPARs (Chen et al., 2000). These data show that γ-8 and Stargazin determine AMPAR stability and synaptic recruitment. Furthermore, the data obtained from γ-8-deficient mice indicate that even strong reductions in overall AMPAR levels do not cause similarly severe reductions in synaptic AMPAR function. This apparent lack of a linear correlation between overall AMPAR levels and AMPAR function at synapses might explain why, in the case of the 4.1G/N double-mutant mice described here, a 20-30% reduction of GluR1 levels at postsynapses does not cause a concomitant reduction of synaptic transmission in the hippocampus.

In summary, the present study indicates that proteins 4.1G and 4.1N are generally dispensable for proper function of glutamatergic

synapses in vivo. Data obtained in in vitro studies on these proteins can therefore not be directly extrapolated to the in vivo situation. It is likely that the lack of phenotypic changes in glutamatergic hippocampal synapses of 4.1G/N double mutants is due to a redundancy of these proteins with other 4.1 isoforms or with other postsynaptic scaffold proteins. This notion is supported by the fact that deletion of the only *Drosophila* 4.1 homologue (coracle), causes the loss of coracle-binding GluRIIA receptors from postsynaptic sites, whereas GluRIIB receptors, whose C-terminus does not bind coracle, are not affected, indicating an important role of 4.1 proteins in glutamate receptor anchoring at invertebrate synapses (Chen et al., 2005). However, whether the same is true for mammalian 4.1 proteins will have to be determined in future genetic studies on mice lacking all 4.1 proteins.

Materials and Methods

Generation of 4.1G/N double-mutant mice
For the generation of the 4.1N and the 4.1G single mutant mouse lines (Thomas and Capecchi, 1987) we used genomic clones that had been isolated from a 129SV mouse genomic λ FIXII library (Stratagene). DNA fragments of these clones were used to construct the targeting vectors (Fig. 1A,D). The linearized DNAs of the 4.1N and 4.1G targeting vectors were electroporated into embryonic stem cells (E14), and colonies were selected with G418 and Ganciclovir. Double-resistant clones were analyzed by Southern blotting (Fig. 1B,E). Clones containing the recombined genes were expanded and injected into mouse blastocysts to obtain highly chimeric mice that transmitted the mutation through the germ line. Germ-line transmission was confirmed by Southern blotting of tail-biopsy genomic DNA. Subsequently, routine genotyping of DNA from tail biopsies was performed by PCR (Fig. 1C,F,G).

In vivo 3D MRI
WT and 4.1G/N double-mutant mice underwent MRI measurements at the age of 3 weeks and 7 months. All measurements were obtained at 2.35 T (Bruker BioSpin). In vivo 3D T1-weighted (FLASH, TR/TE=17/7.58 mseconds, flip angle 25°) and T2-weighted images (FSE, TR/TE=3000/60.95 mseconds, 8 echoes, inter-echo spacing=14.4 mseconds) were acquired with an isotropic resolution of 117 μm and a total measurement time of about 195 minutes per animal. The whole brain volume (excluding brainstem), size of cerebellum and size of lateral ventricles were determined in T1-weighted images by manually drawing respective regions of interests on up to 50 contiguous horizontal MRI sections.

Immunostaining and light microscopic quantification
4-week-old wild-type and 4.1G/N double-mutant mice were deeply anesthetized with tribromoethanol and perfused transcardially with 4% paraformaldehyde in 0.1 M PB (sodium phosphate buffer, pH 7.4). Brains were removed and fixed overnight in 4% paraformaldehyde, cryoprotected in sucrose and frozen on dry ice. Serial sagittal cryostat sections (18 μm thick) were collected on slides and stored at –80°C until used. After blocking in PB containing 5% normal goat serum and 0.25% Triton X-100, the sections were stained using antibodies against VGLUT1/2 (both guinea-pig, 1:10,000, Chemicon) and ProSAP1 (Boeckers et al., 1999) (rabbit, 1:1000). The sections were washed three times in PB and then incubated with Alexa Fluor 488- or Alexa Fluor 555-labelled goat anti-guinea pig or goat anti-rabbit IgG secondary antibodies (Molecular Probes). Coverslips were mounted with Mowiol (Calbiochem). All images were acquired as single layers at zoom factor 2 using a Leica inverted confocal laser scanning microscope (DM IRE 2) with a ×63 oil-immersion lens. To allow for intensity comparisons, the gain and offset were held constant across images. Images were imported into the AnalySIS software (Soft-Imaging Systems) and puncta within the hippocampal CA1 stratum radiatum were quantified by touch-count analysis.

Ultrastructural analyses and quantification
Brains of 3-week-old mice were processed according to standard procedures. In brief, mice were perfused with 4% paraformaldehyde and 0.25% glutaraldehyde in PBS. Sections of hippocampus (2 mm thick) were washed, osmicated for 4 hours (1% OsO_4 in PBS), dehydrated through a graded series of ethanol and propylene oxide, and embedded in Epon by polymerization for 12 hours at 60°C. Ultrathin sections of the CA1 region were cut, contrasted with uranyl acetate and lead citrate, and observed in a LEO 912AB transmission electron microscope (Zeiss). Digital images were taken with a ProScan CCD camera and analyzed with CellP analysis software (Olympus).

RNA isolation, RT-PCR and RNA-ligase-mediated (RLM)-RACE
Total RNA was isolated from WT and 4.1G/N double-mutant whole brains using the RNeasy Lipid Tissue Kit (Qiagen). First-strand cDNA was synthesized with Superscript III (Invitrogen) from adaptor-ligated RNA, which was obtained according to the manual of the FirstChoice RLM-RACE Kit (Ambion). A gene-specific primer or an oligo dT primer was utilized for this purpose. 5′RACE of 4.1N was accomplished according to the manual of the FirstChoice RLM-RACE Kit (Ambion). The 5′RACE was performed using two gene-specific nested primers as the reverse primers and the kit provided nested primers (outer primer and inner primer) as the forward primers. Both PCR reactions (outer and inner PCR) were performed at an annealing temperature of 59°C. The amplified products of two different 5′RACE gene-specific primer combinations were purified using QIAquick Gel Extraction Kit (Qiagen), cloned into pCR2.1TOPO (Invitrogen) and sequenced. The 3′RACE of 4.1N was carried out with two gene-specific nested primers as the forward primers and the nested primers provided with the kit as the reverse primers. 3′RACE PCR products were analyzed as described above for the 5′RACE. The sequences of primers are: first strand synthesis primer, 5′-CGTGGGCGTGGTGGTTTGA-3′; gene-specific 5′ RACE primers,
    5′-TCGGCATCATAGTCACCCAGTTCA-3′; 5′-CCAGAAGGGCATGCGTGA-CAAAG-3′; 5′-TGCGCTCCCGATCCCAGTCT-3′; 5′-GATGCTGGCCTGGTGCT-TCAAC-3′; 5′RACE outer primer, 5′-GCT GAT GGC GAT GAA TGA ACA CTG-3′; 5′RACE inner primer, 5′-CGC GGA TCC GAA CAC TGC GTT TGC TGG CTT TGA TG-3′; gene-specific 3′RACE primers, 5′-CCTCAGTCAGTGAGA-ATCACGATGC-3′; 5′-TGAAGGAGCCCAACAGCAAACT-3′; 3′RACE outer primer, 5′-GCG AGC ACA GAA TTA ATA CGA CT-3′; 3′RACE inner primer: 5′-CGC GGA TCC GAA TTA ATA CGA CTC ACT ATA GG-3′.

Western blotting and preparation of synaptosomal fractions
Synaptosomal fractions were prepared according to published protocols (Nicholls, 1978). For western blot sample preparation, olfactory bulbs, cortices, striata, hippocampi, thalami, hypothalami, colliculi, cerebella, brain stems and spinal cords from adult mouse brains were removed and homogenized in 320 mM sucrose, 5 mM HEPES-NaOH (pH 7.4), 0.1 M EDTA (pH 8.0), 0.1 mM phenylmethylsulfonyl fluoride, 1 μM aprotinin and 0.5 μM leupeptin. After determination of protein concentrations, samples were diluted in SDS-PAGE sample buffer and analyzed according to standard procedures (Laemmli, 1970; Towbin et al., 1992). For western blot detection, the membranes were blocked for 30 minutes in Tris-buffered saline (TBS), 0.1% Tween 20, containing 5% dry milk and 5% goat serum and incubated with specific primary antibodies [anti-4.1G raised against the N-terminus in guinea-pig; monoclonal anti-4.1N (BD Biosciences); anti-4.1N raised against the N-terminus in guinea-pig; rabbit anti-4.1N detecting the CTD; mouse anti-GluR1 C3T (Upstate); rabbit anti-GluR4 (Upstate); rabbit anti-GluR2/3 (Chemicon); mouse anti-NMDA-NR1 M68 (Synaptic Systems)] diluted in blocking buffer, followed by the respective horseradish peroxidase (HRP)-conjugated secondary antibody (Jackson ImmunoResearch). Immunoreactive proteins were visualized by enhanced chemiluminescence (ECL Plus system; Amersham Biosciences). For quantitative western blot analyses, Alexa Fluor 680-coupled secondary antibodies were used and the fluorescently labelled bands were quantified with the Odyssey Infrared imaging system (Li-Cor Biosciences). Statistical analyses were performed using Student's *t*-test.

PSD preparation
3-week-old 4.1G/N double-mutant mice and WT control animals were sacrificed and the hippocampi were isolated. The hippocampi of each animal were homogenized in ten volumes of homogenisation buffer (320 mM sucrose, 20 mM HEPES-KOH (pH 7.4), 5 mM EDTA, 0.1 mM PMSF). The homogenate was centrifuged for 10 min at 1000 *g*. Supernatants S1 were recentrifuged for 10 minutes at 15,000 *g*, and the resulting P2 pellets were resuspended in resuspension buffer (20 mM Tris-HCl pH 7.4, 2 mM EGTA, 1 mM PMSF). Protein concentration was determined by Bradford assay. For solubilization, the protein concentration was set to 2 mg/ml, and Triton X-100 was added to a final concentration of 1%. The samples were sonicated, followed by agitation for 1 hour at 4°C. Extracts were centrifuged at 100,000 *g* for 1 hour. The supernatant is the Triton-soluble fraction. The PSD-pellet (Triton-insoluble fraction) was resuspended in 0.1 volume of 1% SDS, 2 mM EDTA, and 20 mM Tris-HCl (pH 7.4). Then 0.9 volume of resuspension buffer was added and the samples were agitated for 1 hour at 4°C. Protein concentration was determined by BCA assay. 25 μg protein was loaded per lane and analyzed by SDS-PAGE followed by western blotting. Densitometric analysis was carried out using ImageJ software, and the signals were normalized to β-tubulin signals. Significance was determined by Student's *t*-test.

Electrophysiology
WT and 4.1G/N double-mutant mice (3- to 5-weeks old) of both genders were decapitated under anesthesia and the brains were quickly removed. Horizontal hippocampal mouse brain slices (300 μm thick) were prepared in saccharose-based ACSF containing 87 mM NaCl, 1.25 mM NaH_2PO_4, 2.5 mM KCl, 26 mM $NaHCO_3$, 7 mM $MgCl_2$, 0.5 mM $CaCl_2$, 75 mM saccharose and 25 mM glucose. After incubation for 30 minutes at 36°C, slices were transferred to physiological ACSF solution (119 mM NaCl, 1 mM NaH_2PO_4, 2.5 mM KCl, 1.3 mM $MgSO_4$, 2.5 mM $CaCl_2$, 26 mM $NaHCO_3$, 10 mM glucose, saturated with 95% O_2 and 5% CO_2 at pH 7.4) and kept at room temperature. Field potential recordings were performed with low-resistance

patch-clamp electrodes filled with ACSF. Field EPSPs were recorded in stratum radiatum in area CA1. Schaffer collaterals were stimulated with a frequency of 0.05 Hz. Single cell recordings were performed in whole cell patch-clamp mode. Patch-clamp electrodes (electrode resistance 2-5 MΩ) were filled with 117.5 mM Cs-gluconate, 2.5 mM CsCl, 8 mM NaCl, 10 mM HEPES, 10.0 mM TEA, 0.2 mM EGTA, 4 mM Mg-ATP, 0.3 mM Na$_3$GTP and QX-314 2; pH was adjusted to 7.2 with CsOH. Access resistance ranged from 6 to 20 MΩ and was continuously monitored throughout the experiment. Recordings were discarded when the series resistance changed more than 20%. All patch-clamp experiments were done in the presence of the GABA$_A$ receptor-antagonist gabazine (SR 95531, 1 μM; Sigma) and 4 mM MgSO$_4$ and CaCl$_2$. AMPA/NMDA ratios were obtained by evoking single-component EPSCs at –60 mV and a dual-component EPSCs at +40 mV. The NMDA-mediated portion of the dual-component current at +40 mV was measured 100 mseconds after the stimulation artefact. AMPAR-rectification index was determined (in the presence of 40 μM APV) as current amplitude at a holding potential of –60 mV divided by the amplitude at + 40 mV. Miniature EPSCs were recorded in the presence of tetrodotoxin (TTX, 1 μM) and cyclothiazide (100 μM). AMPA-mediated whole-cell currents were obtained by bath application of 100 nM S-AMPA for five minutes in the presence of TTX and cyclothiazide. In field recordings, LTP was induced by four tetani of high-frequency stimulation at 100 Hz for 1 second with 20 second intertrain intervals. The magnitude of LTP was determined by averaging the responses collected during the last 5 minutes of each experiment. Paired-pulse facilitation (P2/P1) in the field and whole-cell recordings was investigated by analysing the ratio of second the first synaptic response. Data are expressed as mean ± s.e.m., and statistical comparison was done by applying Student's t-test (Excel, Microsoft). The significance level was set to $P<0.05$.

References

Barry, M. F. and Ziff, E. B. (2002). Receptor trafficking and the plasticity of excitatory synapses. *Curr. Opin. Neurobiol.* **12**, 279-286.

Beique, J. C. and Andrade, R. (2003). PSD-95 regulates synaptic transmission and plasticity in rat cerebral cortex. *J. Physiol.* **546**, 859-867.

Boeckers, T. M., Kreutz, M. R., Winter, C., Zuschratter, W., Smalla, K. H., Sanmarti-Vila, L., Wex, H., Langnaese, K., Bockmann, J., Garner, C. C. et al. (1999). Proline-rich synapse-associated protein-1/cortactin binding protein 1 (ProSAP1/CortBP1) is a PDZ-domain protein highly enriched in the postsynaptic density. *J. Neurosci.* **19**, 6506-6518.

Bredt, D. S. and Nicoll, R. A. (2003). AMPA receptor trafficking at excitatory synapses. *Neuron* **40**, 361-379.

Cai, C., Coleman, S. K., Niemi, K. and Keinanen, K. (2002). Selective binding of synapse-associated protein 97 to GluR-A alpha-amino-5-hydroxy-3-methyl-4-isoxazole propionate receptor subunit is determined by a novel sequence motif. *J. Biol. Chem.* **277**, 31484-31490.

Chen, K., Merino, C., Sigrist, S. J. and Featherstone, D. E. (2005). The 4.1 protein coracle mediates subunit-selective anchoring of drosophila glutamate receptors to the postsynaptic actin cytoskeleton. *J. Neurosci.* **25**, 6667-6675.

Chen, L., Chetkovich, D. M., Petralia, R. S., Sweeney, N. T., Kawasaki, Y., Wenthold, R. J., Bredt, D. S. and Nicoll, R. A. (2000). Stargazin regulates synaptic targeting of AMPA receptors by two distinct mechanisms. *Nature* **408**, 936-943.

Coleman, S. K., Cai, C., Mottershead, D. G., Haapalahti, J. P. and Keinanen, K. (2003). Surface expression of GluR-D AMPA receptor is dependent on an interaction between its C-terminal domain and a 4.1 protein. *J. Neurosci.* **23**, 798-806.

Conboy, J. G., Chan, J. Y., Chasis, J. A., Kan, Y. W. and Mohandas, N. (1991). Tissue- and development-specific alternative RNA splicing regulates expression of multiple isoforms of erythroid membrane protein 4.1. *J. Biol. Chem.* **266**, 8273-8280.

Collingridge, G. L., Isaac, J. T. and Wang, Y. T. (2004). Receptor trafficking and synaptic plasticity. *Nat. Rev. Neurosci.* **5**, 952-962.

Ehrlich, I. and Malinow, R. (2004). Postsynaptic density 95 controls AMPA receptor incorporation during long-term potentiation and experience-driven synaptic plasticity. *J. Neurosci.* **24**, 916-927.

Elias, G. M., Funke, L., Stein, V., Grant, S. G., Bredt, D. S. and Nicoll, R. A. (2006). Synapse-specific and developmentally regulated targeting of AMPA receptors by a family of MAGUK scaffolding proteins. *Neuron* **52**, 307-320.

Fukata, Y., Tzingounis, A. V., Trinidad, J. C., Fukata, M., Burlingame, A. L., Nicoll, R. A. and Bredt, D. S. (2005). Molecular constituents of neuronal AMPA receptors. *J. Cell Biol.* **169**, 399-404.

Gascard, P., Parra, M. K., Zhao, Z., Calinisan, V. R., Nunomura, W., Rivkees, S. A., Mohandas, N. and Conboy, J. G. (2004). Putative tumor suppressor protein 4.1B is differentially expressed in kidney and brain via alternative promoters and 5′ alternative splicing. *Biochimica et biophysica acta* **1680**, 71-82.

Hayashi, Y., Shi, S. H., Esteban, J. A., Piccini, A., Poncer, J. C. and Malinow, R. (2000). Driving AMPA receptors into synapses by LTP and CaMKII: requirement for GluR1 and PDZ domain interaction. *Science* **287**, 2262-2267.

Kim, C. H., Chung, H. J., Lee, H. K. and Huganir, R. L. (2001). Interaction of the AMPA receptor subunit GluR2/3 with PDZ domains regulates hippocampal long-term depression. *Proc. Natl. Acad. Sci. USA* **98**, 11725-11730.

Laemmli, U. K. (1970). Cleavage of structural proteins during the assembly of the head of bacteriophage T4. *Nature* **227**, 680-685.

Lakso, M., Pichel, J. G., Gorman, J. R., Sauer, B., Okamoto, Y., Lee, E., Alt, F. W. and Westphal, H. (1996). Efficient *in vivo* manipulation of mouse genomic sequences at the zygote stage. *Proc. Natl. Acad. Sci. USA* **93**, 5860-5865.

Lu, D., Yan, H., Othman, T. and Rivkees, S. A. (2004). Cytoskeletal protein 4.1G is a binding partner of the metabotropic glutamate receptor subtype 1 alpha. *J. Neurosci. Res.* **78**, 49-55.

Luthi, A., Chittajallu, R., Duprat, F., Palmer, M. J., Benke, T. A., Kidd, F. L., Henley, J. M., Isaac, J. T. and Collingridge, G. L. (1999). Hippocampal LTD expression involves a pool of AMPARs regulated by the NSF-GluR2 interaction. *Neuron* **24**, 389-399.

Malenka, R. C. and Bear, M. F. (2004). LTP and LTD: an embarrassment of riches. *Neuron* **44**, 5-21.

Marfatia, S. M., Leu, R. A., Branton, D. and Chishti, A. H. (1995). Identification of the protein 4.1 binding interface on glycophorin C and p55, a homologue of the Drosophila discs-large tumor suppressor protein. *J. Biol. Chem.* **270**, 715-719.

Migaud, M., Charlesworth, P., Dempster, M., Webster, L. C., Watabe, A. M., Makhinson, M., He, Y., Ramsay, M. F., Morris, R. G., Morrison, J. H. et al. (1998). Enhanced long-term potentiation and impaired learning in mice with mutant postsynaptic density-95 protein. *Nature* **396**, 433-439.

Nakagawa, T., Futai, K., Lashuel, H. A., Lo, I., Okamoto, K., Walz, T., Hayashi, Y. and Sheng, M. (2004). Quaternary structure, protein dynamics, and synaptic function of SAP97 controlled by L27 domain interactions. *Neuron* **44**, 453-467.

Nicholls, D. G. (1978). Calcium transport and porton electrochemical potential gradient in mitochondria from guinea-pig cerebral cortex and rat heart. *Biochem. J.* **170**, 511-522.

Nicoll, R. A., Tomita, S. and Bredt, D. S. (2006). Auxiliary subunits assist AMPA-type glutamate receptors. *Science* **311**, 1253-1256.

Ohara, R., Yamakawa, H., Nakayama, M. and Ohara, O. (2000). Type II brain 4.1 (4.1B/KIAA0987), a member of the protein 4.1 family, is localized to neuronal paranodes. *Brain Res. Mol. Brain Res.* **85**, 41-52.

Ohno, N., Terada, N., Tanaka, J., Yokoyama, A., Yamakawa, H., Fujii, Y., Baba, T., Ohara, O. and Ohno, S. (2005). Protein 4.1 G localizes in rodent microglia. *Histochem. Cell Biol.* **124**, 477-486.

Ramez, M., Blot-Chabaud, M., Cluzeaud, F., Chanan, S., Patterson, M., Walensky, L. D., Marfatia, S., Baines, A. J., Chasis, J. A., Conboy, J. G. et al. (2003). Distinct distribution of specific members of protein 4.1 gene family in the mouse nephron. *Kidney Int.* **63**, 1321-1337.

Rouach, N., Byrd, K., Petralia, R. S., Elias, G. M., Adesnik, H., Tomita, S., Karimzadegan, S., Kealey, C., Bredt, D. S. and Nicoll, R. A. (2005). TARP gamma-8 controls hippocampal AMPA receptor number, distribution and synaptic plasticity. *Nat. Neurosci.* **8**, 1525-1533.

Rumbaugh, G., Sia, G. M., Garner, C. C. and Huganir, R. L. (2003). Synapse-associated protein-97 isoform-specific regulation of surface AMPA receptors and synaptic function in cultured neurons. *J. Neurosci.* **23**, 4567-4576.

Schnell, E., Sizemore, M., Karimzadegan, S., Chen, L., Bredt, D. S. and Nicoll, R. A. (2002). Direct interactions between PSD-95 and stargazin control synaptic AMPA receptor number. *Proc. Natl. Acad. Sci. USA* **99**, 13902-13907.

Setou, M., Seog, D. H., Tanaka, Y., Kanai, Y., Takei, Y., Kawagishi, M. and Hirokawa, N. (2002). Glutamate-receptor-interacting protein GRIP1 directly steers kinesin to dendrites. *Nature* **417**, 83-87.

Shen, L., Liang, F., Walensky, L. D. and Huganir, R. L. (2000). Regulation of AMPA receptor GluR1 subunit surface expression by a 4. 1N-linked actin cytoskeletal association. *J. Neurosci.* **20**, 7932-7940.

Thomas, K. R. and Capecchi, M. R. (1987). Site-directed mutagenesis by gene targeting in mouse embryo-derived stem cells. *Cell* **51**, 503-512.

Towbin, H., Staehelin, T. and Gordon, J. (1992). Electrophoretic transfer of proteins from polyacrylamide gels to nitrocellulose sheets: procedure and some applications: 1979. *Biotechnology* **24**, 145-149.

Trinidad, J. C., Thalhammer, A., Specht, C. G., Lynn, A. J., Baker, P. R., Schoepfer, R. and Burlingame, A. L. (2008). Quantitative analysis of synaptic phosphorylation and protein expression. *Mol. Cell Proteomics.* **7**, 684-696.

Vandenberghe, W., Nicoll, R. A. and Bredt, D. S. (2005). Interaction with the unfolded protein response reveals a role for stargazin in biosynthetic AMPA receptor transport. *J. Neurosci.* **25**, 1095-1102.

Yamakawa, H. and Ohara, O. (2000). Comparison of mRNA and protein levels of four members of the protein 4.1 family: the type II brain 4.1/4.1B/KIAA0987 is the most predominant member of the protein 4.1 family in rat brain. *Gene* **248**, 137-145.